Indian Journal of Pure & Applied Physics
Vol. 63, July 2025, pp. 648-665
DOI: 10.56042/ijpap.v63i7.19736

Numerically modelled evaluation of all optical RZ OOK conversion to higher order M–QAM format conversion using photic fiber nonlinearity

Deepak Sahu & Chakresh Kumar*

University School of Information, Communication & Technology, Guru Gobind Singh Indraprastha University, New Delhi 110 078, India

Received: 15 May 2025; accepted: 5 June 2025

This study shows how to convert all-optical RZ-OOK to 8QAM code using a nonlinear photonic looped mirror (NOLM), which takes advantage of power-dependent phase alteration and interferometry. The methodology uses Gaussian-pulse RZ-OOK transmissions at 20-30 Gbps to study the effect of duty cycles (20-66%) and nonlinear components (γ = 1.0-2.5 $W^{-1}km^{-1}$) on constellation formation. Key findings show that a 33-50% duty cycle with γ = 1.5-2.0 produces identifiable 8QAM constellations, with "1" bits forming four phase-rotated high-amplitude regions and "0" bits clustering at the origin. The system is unique in that it allows for DSP-free higher-order control conversion, which is useful for minimal latency optical connection networks. However, performance is constrained by nonlinear interference correlation and phase asymmetry.

Keywords: Self-phase modulation, Higher order modulation format, On-off keying, Phase shifts modulation, LAN networks

1 Introduction

The increasing demand for high-speed and flexible optical communication systems has driven the development of advanced modulation format conversion techniques. Among these, the conversion from Return-to-Zero On-Off Keying (RZ-OOK) to 8-ary Quadrature Amplitude Modulation (8QAM) is particularly significant due to the need for efficient data transmission in modern optical networks. The research investigates ways for boosting intra-datacentre optical hyperlinks beyond one Tb/s. It contrasts two major strategies: Strength Modulation-Direct Detection (IM-DD) using PAM4/PAM6/ PAM8, and Heterogeneous Detection with PM-QAM. The work proposes Flexible PAM for dynamic modulation flexibility and presents low-power coherent DSP solutions in addition to unique phase-noise resistant modulation forms. A rigorous execution, dominance, and adaptability comparison demonstrates coherent technology's benefits for future scaling, particularly beyond 3 km and towards 4.0 Tb/s.[1] The study introduces and tests an all-optical architecture for data centre interconnects (DCI) with dynamic reconfiguration. It demonstrates that sorting and amplifier fluctuations have little effect on signal quality, allowing reconfiguration in mere milliseconds with no BER loss. When compared to typical electrical switching, this strategy can save greatly on cost, power, and area.[2] The document suggests three expandable inert optical topologies for information centres that use arrayed wavefront grating routers (AWGRs) to conserve money as well as energy. The PODCA-S, PODCA-M, and PODCA-L topologies offer high throughput (100%) and low packet latency (sub 25μs) by passing costly customised wavelength converters and focussing on quick programmable transmitters and inert optical components. Models reveal that PODCA greatly surpasses electrical data centre networks in terms of energy efficiency and expense while saving at least 70% on power and 45% on expenditures.[3] The research describes a new versatile, all-optical method for interconverting multiple 8QAM signal codecs – square, standard, and star-shaped 8QAM – utilising a pump-assisted NOLM, which is quantitatively verified for the first occasion. The suggested arrangement separates input 8QAM signals into clockwise and anticlockwise routes inside a NOLM, which allows them undergo self-phase modulation (SPM) and cross-phase modulation (XPM), enabling coherent recombination to generate fresh signal formats. Dynamic all-optical structure interconversion between square-8QAM, star-8QAM, and standard-8QAM can be handled by simply adjusting the input signal and pump power, minimising the need for complex discrete optical

*Corresponding author: E-mail: chakreshk@ipu.ac.in

components. Mathematical models demonstrate that the constellation, eye diagrams, Error Vector Magnitude (EVM), and Bit Error Rate (BER) are maintained with the least penalty. The study illustrates transitioning 20 Gbps square-8QAM impulses to 10 Gbps QPSK signals using the identical NOLM framework, resulting in considerable OSNR increases (~6dB). This increases the system's versatility by supporting optical format down-conversion, which is important for a wide range of optical network types. This suggested pump-assisted NOLM system is characterised as more steady (less sensitive to external factors such as temperature and movement) than earlier nonlinear MZI approaches, and it shows significant potential for execution in optical interfaces to adaptable interconnect distinct sections of the network using various modulation formats. Ultimately, this investigation represents a major advance towards low-latency, high-capacity, and programmable optical network structures.[4] The paper offers an all-optical technique to switch QPSK signals into PAM4 layout to allow smooth linking among long-haul and data-center networks. Employing two nonlinear instances (relying on PPLN wave paths), a QPSK indicate is first coupled, phase-rotated, and then cohesively paired with a CW pump to map phase insights into intensity heights identified by a photo diode. The exploratory results indicate prosperous 10–20 Gbit/s QPSK-to-PAM4 transformation with clear eye illustrations and suitable BER execution. The system also reveals adjusted wavelength switching, showing agility for data-center activity wavelengths that are like 850 nm and 1310 nm. The tackle eliminates multifaceted coherent receivers, backing less complicated direct-detection-based layouts.[5] The research offers a unique all-optical technique which employs phase-sensitive augmentation in extremely nonlinear fibre (HNLF) to convert an individual 20-Gbps 8PSK signal into two 10-Gbps QPSK signals without compromising data. To generate phase-locked QPSK outputs, the approach employs two concurrent phase-squeezing mechanisms that make use of FWM and intrusion. Mathematical calculations indicate a ~4.7dB boost in OSNR at a BER limit of 3.76×10^{-3} compared to that initial 8PSK signal. EVM and BER research show that the switched QPSK signals maintain superior quality under a variety of OSNR situations. Services supported by the converter include traffic training, private communication, and interoperability between optical networks. This work improves adaptability, safeguards, and spectrum effectiveness of stretchy optical networks (aeons).[7] The study presents a PSA-based framework for converting 2D QAM signals to 1D PAM signals. It shows seven different sorts of changes, notably QPSK-to-PAM4 and 8QAM-to-PAM8, utilising two techniques: constellation compression and multi-level vector mobility. The device allows for configurable management of eye diagrams by altering the PSA gain axis. Experimental findings reveal that with input OSNRs of 20-30 dB, transformed PAM signals achieve high-quality BER and OSNR efficiency, making them appropriate for connecting long-haul cohesive networks with short-reach immediate identification systems. This technology enables adaptable optical format conversion, signal moulding, and optical network interface.[8] An all-optical organisation and de-aggregation strategy for one 8-ary quadrature amplitude modulation (8QAM) transmission and three binary phase shift keying (BPSK) outputs is laid out and conceptually simulated using nonlinear effects in high nonlinear fibre (HNLF). The input 8QAM signal is de-aggregated into three BPSK signals employing self-phase modulation (SPM), cross-phase modulation (XPM), four wave mixing (FWM), and the parameter amplification (PA) effect. For purposes of assessing the scheme's performance, the error vector magnitude (EVM) and bit error ratio (BER) of the 8QAM and BPSK signals have been calculated before and after de-aggregation and aggregation sequentially. The strategy can be used in network nodes to connect networks that use 8QAM and BPSK signals, accordingly.[9] The research presents a customisable all-optical system for transforming star-8QAM signals into multiple QPSK signals by combining a nonlinear Mach-Zehnder Interferometer (MZI) with hierarchical pump-assisted NOLMs. The system de-aggregates a star-8QAM into three distinct kinds of QPSK signals and then re-aggregates into 8QAM using coherent addition, which facilitates dynamic optical linkages between different network topologies. It also converts codecs between bipolar PAM4 to BPSK/QPSK and 16QAM to dual QPSK signals by employing phase-sensitive amplification (PSA). Modelling exhibit clear constellation recuperation, OSNR gains, and BER enhancements emphasising superior noise immunity and adaptation. This scheme optimises stretchy optical networks, optical gateways, and encrypted communication of information.[10] The article describes

an innovative approach for transforming one type of data signal, non-return-to-zero on-off-keying (NRZ-OOK), into another, return-to-zero 16 quadrature amplitude modulation (RZ-16QAM). The process of conversion is necessary for better communication of information in optical connections. The suggested approach employs a nonlinear optical loop mirror (NOLM) in conjunction with a 1:2 coupler setup. This configuration allows the conversion to take place entirely optically, eliminating the need for electrical analysing, which might slow down the signal. The conversion process was tested scientifically at a speed of ten gigabits per second (10Gs/s). The research also analyses the impact of amplified spontaneously generated (ASE) noise, which happens when impulses are enhanced. This distortion can damage the quality of the converted 16QAM signal, especially its phase. The authors present an analytical investigation of how this noise affects the effectiveness of the translated signal.[11] The major goal is to investigate a method for converting various optical signal formats, particularly Return-to-Zero (RZ) and Carrier-Suppressed Return-to-Zero (CSRZ), to Non-Return-to-Zero (NRZ) format. This transformation is critical to increasing effectiveness and scalability of optical communication systems. The study takes an all-optical method, which indicates that the conversion process has no reliance on electronic elements. This is essential because it has the ability to improve the rate of data transfer while also minimising congestion. The research investigation emphasises on multi-channel settings, demonstrating that the approach can manage many data flows concurrently. The article discusses the successful outcome of the suggested plan in achieving the intended format conversion. It is suggested by the findings that further exploration into this all-optical conversion technique could lead to advancements in optical network design and implementation. Future research directions may be proposed by the paper, such as optimizing the conversion process or exploring additional formats that could benefit from similar techniques.[12] The study presents a strategy for aggregating optical signals from OOK to 8QAM. This is crucial because it increases the potential as well as effectiveness of optical connections, which are critical to modern communication infrastructure. The method of operation uses a 10G Baud rate and an interface for combining three OOK channels into a single 8QAM channel. This procedure is extensively analysed, highlighting the technical components of the aggregation. Numerous performance metrics have been evaluated in the article, notably constellation diagrams, eye diagrams, and bit error rate (BER) for OOK, PAM4, and 8QAM signals. These specifications are critical when measuring the calibre as well as durability of sent signals. The findings highlight the significance of optical aggregation as an enabler for the advancement of optical connections. This method, by allowing for more expansive capacity and improved data transfer, has the potential to greatly develop optical communication systems. While the paper focusses on the existing execution, it provides a foundation for future research into optimising the aggregation process and investigating new modulation forms. This could result in even larger increases to optical network efficiency and capacity in the future.[13] The fundamental goal of the study is to provide a method for converting among several modulation formats, notably Quadrature Phase Shift Keying (QPSK), On-Off Keying (OOK), and 8-Quadrature Amplitude Modulation (8QAM). The process of conversion is critical in optical communication systems for increasing transmission of information efficiency and versatility. The authors employ all-optical methods to accomplish modulation style transformation. This entails harnessing nonlinear phenomena that exist in semiconductor optical amplifiers (SOAs) and optical threshold devices. All of these elements play an important role in modulating light signals to ensure proper data flow. The study concludes that the proposed method delivers error-free format conversion. This implies that the confidentiality of the data is preserved during the conversion procedure, which is an important feat in optical networking.[14] The primary purpose of this study is to create a mechanism for converting optical modulation codecs. It emphasises on transforming On-Off Keying (OOK) and Quadrature Phase Shift Keying (QPSK) to 8-Quadrature Amplitude Modulation (8QAM) utilising particular methods in a semiconductor optical amplifier (SOA). The study suggests that the calculated Bit Error Rate (BER) results show that the suggested approach is capable of converting from OOK and QPSK to 8QAM. It suggests that the new approach is suitable for practical use in optical networks of communication. The effective conversion to 8QAM is crucial because it has the ability to increase both the capacity and the effectiveness of optical communication systems. The method's use of a single SOA may help facilitate both

the creation and execution of such systems.[15] The study describes an all-optical format conversion (AOFC) technique that uses nonlinear phenomena in high nonlinear fibre (HNLF) to transform star-8QAM signals. This technology is important for improving networks of optical communications because it enables various modulation formats to be used interchangeably at optical hubs. The system enables for customisation of the amplitude ratio (AR) between the outer and inner rings of the accumulated star-8QAM signal. This modification is made feasible by altering the energy levels of the QPSK and OOK signals, which can result in the production of additional modulation formats. The reliability of the AOFC method is assessed by comparing the error vector magnitude (EVM) and bit error ratio (BER) of the star-8QAM signals before and after the AOFC approach.[16] The work highlights the utilisation of nonlinear effects in diverse mediums, including χ^2 and χ^3 nonlinear media. These impacts are critical for the modulation format transformation procedure, which is required for improved broadcast quality in optical connections. It describes a variety of nonlinear mediums used in the conversion process, including: High Nonlinear Fibre (HNLF) Semiconductor Optical Amplifier (SOA) using Periodically-Poled Lithium Niobate. The study illustrates how different modulation formats are appropriate for different types of optical networks. Factors that affect this allocation include: Transmission Range, Cost, consumed energy, Sensitivity for acquiring devices Length of optical networks. The study of MFC for 8QAM signals has been considered essential, especially at network nodes that are intermediary. These nodes are vital for interconnecting diverse networks of optics, such as short-reach and long-haul networks, which enables reliable information transmission.[17] The work looks into the use of phase responsive augmentation (PSA) in highly nonlinear fibre (HNLF) for programmable all-optical format conversion. This is primarily intended to improve optical information centre networks, which necessitate effective data handling and transport technologies. The mathematical framework is validated using computer simulations. These simulations aid in determining the efficacy of the proposed methodologies and provide insight into their practical applications. The technique suggested supports adjustable all-optical format conversion. It can transform a 16QAM (Quadrature Amplitude Modulation) signal into two QPSK (Quadrature Phase Shift Keying) signals, or an 8QAM signal into one QPSK signal and one binary phase shift keying signal. This versatility is critical for adjusting to changing data transfer requirements.[18]

2 Mathematical Analysis

2.1 RZ-OOK to 8QAM Conversion Employing NOLM

RZ-OOK (Return-to-Zero On-Off Keying) is a straightforward modulation format that represents each bit with a short optical pulse (for '1') or no pulse (for '0') whereas 8-QAM (8-Quadrature Amplitude Modulation) is a higher-order modulation format that uses amplitude and phase fluctuations to convey three bits per symbol. The challenge for format conversion is that OOK contains one bit per symbol, but only in amplitude while 8-QAM carries 3 bits per symbol, combining both amplitude and phase. Thus, there is a need to translate OOK data into the phase and amplitude of a coherent optical signal, which is a far more complex process. The Nonlinear Optical Loop Mirror (NOLM) is an interferometric device where two counter-propagating waves interact while undergoing nonlinear phase shifts caused by the Kerr phenomenon within a fibre loop. Pump-assisted NOLM uses an external strong pump burst to create cross-phase modulation (XPM) on the signal that is cycling throughout the loop. Thus, the signal's phase and amplitude can be modified entirely visually. The XPM-induced phase changes are proportional to the pump pulse intensity. The aim is to use pump pulses to induce the intended phase shifts on OOK pulses. Amplitude modulation is accomplished by adjusting the interference between clockwise and anticlockwise pulses in the loop. Following the NOLM, photonic phase along with amplitude are modulated simultaneously to produce 8-QAM symbols. The data signal $S_{ook}(t)$ is a RZ-OOK signal, which consists of optical pulses encoding '1' and '0'. Pump pulses are intense short pulses $P_{pump}(t)$ synchronised with RZ-OOK pulses. They are precisely engineered to control phase. The pump is driven by information, which implies that its power and timing are altered determined by the desired 8-QAM constellation positions. Signal and pump propagate across the NOLM's fibre loop. Owing of the Kerr nonlinearity, the signal undergoes a nonlinear phase modification as shown in Eq. (1).

$$\Delta\phi_{x-phase} = 2\gamma l_{eff} P_{pump} \quad \ldots (1)$$

γ being the non-linear coefficient of the fiber, l_{eff} is the effective length of the fiber $l_{eff} = \left(1 - \exp\left(-\alpha l\right)\right)$ given that α is the attenuation constant and P_{pump} is the pump pulse power. The NOLM has a pair of directions: clockwise (CW) and Anticlockwise (CCW) direction. Both sides encounter various XPM-induced phase shifts dependent on

$$\zeta_{out} = \zeta_{CW} \exp\left(i\Delta\phi_{cw}\right) + \zeta_{C-CW} \exp\left(i\Delta\phi_{c-cw}\right) \quad \ldots (2)$$

the pump, resulting in a sequence of interference at the point of exit. The resultant electrical field ζ_{out} at the output point is given by Eq. (2). Interference can be constructive (bright port) if the phase difference is close to zero, or destructive (dark port) if it is close to π. The relative phase shifts can be precisely controlled employing pump power and timing to engineer both the amplitude and phase of the output. In mathematical form input RZ-OOK

$$S_{ook}\left(t\right) = \sum_{k} a_k \, p\left(t - kT\right) \quad \ldots (3)$$

signal can be represented as shown in Eq. (3), where $a_k \in \{0,1\}$, $p\left(t\right)$ is pulse shape and T is bit period. For a single RZ pulse overlapping a pump pulse change in phase is given by Eq. (4), if $P_{pump}\left(t\right)$ symbolizes a strong short pulse

$$\Delta\phi_{x-phase} = 2\gamma l_{eff} \left|P_{pump}\left(t\right)\right|^2 \quad \ldots (4)$$

given by Eq. (5) then change in phases shift in modified form will be represented as given by Eq. (6). Here peak

$$P_{pump}\left(t\right) = p_o \exp\left\{-\left(t^2/2\sigma_{pump}^2\right)\right\} \quad \ldots (5)$$

$$\Delta\phi_{x-phase} = 2\gamma l_{eff} \, p_o^2 \exp\left\{-\left(t^2/\sigma_{pump}^2\right)\right\} \quad \ldots (6)$$

phase shift occurs at $t = 0$. Further assuming coupler to equal splitting by having ratio of 50:50 has output electrical field at exit given by Eq. (7) from which it can be inferred that both amplitude and phase of the output depends on $\Delta\phi_{x-phase}\left(t\right)$ also Higher XPM results in a bigger phase shift and different amplitude output after interference.

$$\zeta_{out}\left(t\right) = \zeta_{input}\left(t\right)\left\{\cos\left(\Delta\phi_{x-phase}\left(t\right)/2\right) + i\sin\left(\Delta\phi_{x-phase}\left(t\right)/2\right)\right\} \quad \ldots (7)$$

Pump-assisted NOLM introduces nonlinear phase changes via cross-phase modulation (XPM). To generate 8QAM, the optical carrier must undergo both amplitude and phase modulation. The nonlinear interaction is controlled using several ways to provide accurate phase and amplitude control. As a result, different approaches evolved centred on: pump design (amplitude, phase, shape, timing), loop asymmetry (power imbalance between CW and CCW pathways), Fibre qualities include nonlinearity γ, dispersion D, and polarisation management, Control of bias phase shift. Let Signal input field and pump field is given by Eqs (8–9). The pump inside the HNLF

$$\zeta_{sig}\left(t\right) = a_{o,sig} \exp\left(i\phi_{o,sig}\left(t\right)\right) \quad \ldots (8)$$

$$\zeta_{pump}\left(t\right) = a_{o,pump} \exp\left(i\phi_{o,pump}\left(t\right)\right) \quad \ldots (9)$$

(NOLM loop) causes a nonlinear phase shift on the signal, which is $\Delta\phi_{x-phase} = 2\gamma l_{eff} \left|\zeta_{pump}\left(t\right)\right|^2$. Thus, signal field after XPM is given by Eq. (10). The NOLM interferometric output is determined as shown in Eq. (11) where $\Delta\phi_{x-phase}\left(t\right)$ represents the phase difference between CW and CCW arms caused by pump-induced XPM. If there is loop asymmetry (power difference between CW and CCW), the output translates to Eq. (12) where $r \neq 0.5$. This imbalance results in amplitude modulation, which, when paired with phase shift, produces complicated 8-QAM points.

$$\zeta'_{sig}\left(t\right) = a_{o,sig}\left(t\right) \exp\left\{i\left(\phi_{o,sig}\left(t\right) + \Delta\phi_{x-phase}\left(t\right)\right)\right\} \quad \ldots (10)$$

$$\zeta_{out}\left(t\right) = \zeta'_{sig}\left(t\right)\left[1 - \exp\left(i\Delta\phi_{x-phase}\left(t\right)\right)\right]/2 \quad \ldots (11)$$

$$\zeta_{out}\left(t\right) = \sqrt{r}\,\zeta_{CW}\left(t\right) + \sqrt{1-r}\,\zeta_{C-CW} \quad \ldots (12)$$

First method is Single Pump, Pulse Shaping Technique utilizes the concept to use a single pump pulse. Change the pump pulse power and temporal form to produce distinct phase shifts in the signal at different times. Mechanism involved is that XPM-induced phase shifts affect distinct sections of the signal. In addition to NOLM asymmetry, distinct amplitudes are generated. Pump intensity profile can

be represented as shown in Eq. (13) where $f(t)$ is a tailored temporal shape (e.g., Gaussian, sin*c*, shaped pulses). The resultant phase shift induced will be given as $\Delta\phi_{x-phase}(t) = 2\gamma l_{eff} p_o f(t)$. The result obtained is that different regions of the signal acquire different

$$\left|\zeta_{pump}(t)\right|^2 = p_o f(t) \quad \ldots (13)$$

phase shifts and output amplitudes. Second method is dual pump method where two coordinated pump pulses of varying frequencies and strengths are injected resulting is generation of various levels of amplitudes and phase shift simultaneously. The first pump causes an elementary XPM phase transition. The subsequent pump generates extra modulation. The combined impact amounts constellation points for 8QAM. This approach offers higher degree of freedom resulting in more manageable 8QAM points spacing. Let the two pump fields be represented by Eqs (14–15) resulting in combined XPM-induced phase shift represented in Eq. (16) clearly stating that now

$$\zeta_{p1}(t) = a_{o,p1}(t)\exp\left(i\phi_{p1}(t)\right) \quad \ldots (14)$$

$$\zeta_{p2}(t) = a_{o,p2}(t)\exp\left(i\phi_{p2}(t)\right) \quad \ldots (15)$$

$$\Delta\phi_{x-phase}(t) = 2\gamma l_{eff}\left(\left|\zeta_{p1}(t)\right|^2 + \left|\zeta_{p2}(t)\right|^2\right) \quad \ldots (16)$$

two controlling knobs (pumps) available for phase modulation. Thirdly Phase-Biased Asymmetric NOLM method is there which introduces a static phase bias inside NOLM loop. The NOLM's shift function is altered to provide more nonlinear behaviour, and a calculated initial phase difference among the CW and CCW channels is added. Pump XPM naturally produces both phase as well as amplitude modulation. This approach holds advantages of robust control over phase shifts and good stability after calibration. Mathematically an induced static bias effect is represented in Eq. (17) where $\zeta'_{sig}(t)$ is mentioned in Eq. (10). Fourthly Polarization-Division Multiplexed

$$\zeta_{out}(t) = \zeta'_{sig}(t)\left[1 - \exp i\left\{\left(\Delta\phi_{x-phase}(t)\right) + \phi_{bias}\right\}\right]\Big/\sqrt{2} \quad \ldots (17)$$

Pumping incorporates using pumps at different polarizations. Polarisation control affects XPM effectiveness as XPM is polarisation sensitive. Pump polarisation angles control the extent that phase shift is created. This approach provides fine-grained control of modulation and can extend to even higher formats (16QAM, etc.). As Pump-induced XPM efficiency depends on relative polarization hence mathematically for co-polarized and cross- polarized pumps XPM phase shift is given by Eqs (18) & (19) respectively. Lastly there is Time-Multiplexed

$$\Delta\phi_{x-phase}(t) \propto 2\gamma\left|\zeta_{pump}(t)\right|^2 \quad \ldots (18)$$

$$\Delta\phi_{x-phase}(t) \propto \gamma\left|\zeta_{pump}(t)\right|^2 \quad \ldots (19)$$

Pump Pulses approach where sequential pump pulses are sent, each pulse inducing a controlled phase shift at different times. In this mechanism signal connects with pump impulses at various moments. Each contact corresponds to a distinct section of the 8QAM constellation. As pump pulses are launched sequentially phase shifts applied at distinct times are given as shown in Eq. (20) where t_k is central time of kth pump pulse. Each pump pulse modifies particular signal bits into the necessary 8-QAM points. Now let us discuss the mathematical

$$\Delta\phi_{x-phase}(t) = \sum_k 2\gamma l_{eff}\left|\zeta_{pump,k}(t - t_k)\right|^2 \quad \ldots (20)$$

representation of RZ-OOK ➔ 8QAM via Pump-Assisted NOLM. The input RZ-OOK signal can be represented as shown in Eq. (21) where $e_{o,sig}$ is the amplitude (takes value 0 or $e_{o,sig}$) depending on bit '0' or '1' and $\phi_{sig}(t)$ is the initial phase usually 0 for OOK. Since the input pulse considered is RZ–OOK the pulse shape is typically

$$\zeta^{in}_{sig}(t) = e_{o,sig}(t)\exp\left(i\phi_{sig}(t)\right) \quad \ldots (21)$$

Gaussian mathematically represented as presented in Eq. (22) where b_k belongs to (0,1) is the kth data bit '0' or '1', T_b is the bit duration and σ is the pulse width parameter typically $\sigma \ll T_b$. Further the pump pulse field is given in Eq. (9). As basically a pump is strong synchronized pulse, Gaussian or flat-top hence its magnitude is given as shown in Eq. (23) where t_{pump} is

the pump pulse timing and σ_{pump} is the pump pulse width. Within the nonlinear optical fibre (NOLM loop), the pumping mechanism triggers XPM on the input signal. The XPM-induced

$$e_{o,sig}(t) = e_o \sum_k b_k \exp\left\{-\left(t - kT_b\right)^2 / 2\sigma^2\right\} \quad \ldots (22)$$

$$a_{o,pump}(t) = a^o_{pump} \exp\left\{-\left(t - t_{pump}\right)^2 / 2\sigma_{pump}{}^2\right\} \quad \ldots (23)$$

nonlinear transition of phase in the signal as shown in Eq. (24). So, the signal post XPM turns into as in Eq. (10). Since $\phi_{o,sig}(t) \approx 0$ for OOK it can be simplified into Eq. (25). Within the NOLM, the field separates into clockwise (CW) and anticlockwise (CCW) orientations. The CW field picks up the pump-induced XPM phase shift, CCW field sees either no pump or a separate pump depending on the design. A numerical model of CW field and CCW

$$\Delta\phi_{x-phase} = 2\gamma l_{eff} \left|a_{o,pump}(t)\right|^2 \quad \ldots (24)$$

$$\zeta'_{sig}(t) = a_{o,sig}(t) \exp\left\{i\left(\Delta\phi_{x-phase}(t)\right)\right\} \quad \ldots (25)$$

is given in Eqs (26–27) where r is the splitting ratio. Thus, after recombination the total output field is presented in Eq. (27). Now substituting the values Eq. (25) in Eq. (27) the transformation is presented in Eq. (28). This is the important field for amplitude and phase modulation. In case of $\Delta\phi_{x-phase}(t)$ being very small using first order Taylor

$$\zeta_{CW}(t) = \sqrt{r}\zeta'_{sig}(t) \quad \ldots (25)$$

$$\zeta_{C-CW}(t) = \sqrt{1-r}\zeta^{in}_{sig}(t) \quad \ldots (26)$$

$$\zeta_{out}(t) = \sqrt{r}\zeta'_{sig} + \sqrt{1-r}\zeta^{in}_{sig}(t) \quad \ldots (27)$$

$$\zeta_{out}(t) = a_{o,sig}(t)\left[\sqrt{r}\exp\left\{i\left(\Delta\phi_{x-phase}(t)\right)\right\} + \sqrt{1-r}\right] \quad \ldots (28)$$

expansion $\exp\left\{i\left(\Delta\phi_{x-phase}(t)\right)\right\} = 1 + i\left(\Delta\phi_{x-phase}(t)\right)$, approximate value of $\exp\left\{i\left(\Delta\phi_{x-phase}(t)\right)\right\}$ is substituted in Eq. (28) resulting into Eq. (29). Thus, the output signal has a modified amplitude proportional to $\sqrt{r} + \sqrt{1-r}$ as shown as A and a phase component proportional to $\Delta\phi_{x-phase}(t)$ shown as B. If a static phase bias ϕ_{bias} is applied to one arm, then output becomes as presented in Eq. (30). If $\phi_{bias} = \pi/4$ linearized conversion is obtained which is crucial for 8QAM generation. Expanding Eq. (30) it is modified to Eq. (31). Thus, Global phase rotation

$$\zeta_{out}(t) \approx a_{o,sig}(t)\left[\sqrt{r}\left\{1 + i\left(\Delta\phi_{x-phase}(t)\right)\right\} + \sqrt{1-r}\right]$$

$$\zeta_{out}(t) \approx a_{o,sig}(t)\left[\underbrace{\sqrt{r} + \sqrt{1-r}}_{A} + \underbrace{i\sqrt{r}\Delta\phi_{x-phase}(t)}_{B}\right] \quad \ldots (29)$$

$$\zeta_{out}(t) = a_{o,sig}(t)\left[\sqrt{r}\exp\left\{i\left(\Delta\phi_{x-phase}(t) + \phi_{bias}\right)\right\} + \sqrt{1-r}\exp\left(i\phi_{bias}\right)\right] \quad \ldots (30)$$

$$\zeta_{out}(t) = a_{o,sig}(t)\exp\left(i\phi_{bias}\right)\left[\sqrt{r}\exp\left\{i\left(\Delta\phi_{x-phase}(t)\right)\right\} + \sqrt{1-r}\right] \quad \ldots (31)$$

$\exp\left(i\phi_{bias}\right)$ (It doesn't affect constellation shape) and the relative phase induced by $\Delta\phi_{x-phase}(t)$ causes the spread into multiple constellation points. Different levels of $\Delta\phi_{x-phase}(t)$ produce different complex field values, corresponding to 8QAM points. For e.g., small $\Delta\phi_{x-phase}(t)$ leads to small imaginary part ⇒ closer to real axis and larger $\Delta\phi_{x-phase}(t)$ results in larger imaginary part ⇒ moves up/down. Amplitude variations are introduced due to power imbalance $r \neq 0.5$ results in 4 amplitudes×2 phases ⇒ 8 constellation points. If multibit transmission is considered the total output field for bit sequences gets transformed into Eq. (32) where, $\Delta\phi_{x-phase}(t)$ now depends on the pump pulses and timing. Thus, the complete RZ-OOK sequence is converted to an 8-QAM symbol stream.

$$\zeta_{out}(t) = e_o \sum_k b_k \exp\left\{-\left(t - kT_b\right)^2 / 2\sigma^2\right\}$$
$$\exp\left(i\phi_{bias}\right)\left[\sqrt{r}\exp\left\{i\left(\Delta\phi_{x-phase}(t)\right)\right\} + \sqrt{1-r}\right] \quad \ldots (32)$$

Now further a mathematical modelling of working concept of Nonlinear Optical Loop Mirror (NOLM) is analysed. An elementary setup of NOLM comprises of *firstly* a 3dB coupler or a slightly asymmetric coupler $r:(1-r)$, *secondly* a fiber loop constructed as highly nonlinear medium and *lastly* a pump pulse

injected either into the loop or counter-propagating. In the loop the signal splits into two parts clockwise wave $\zeta_{CW}(t)$ and counter clockwise wave $\zeta_{C-CW}(t)$. Both of these surges experienced XPM effects (different for CW and CCW paths if pump injected asymmetrically) and Self-Phase Modulation (SPM) (usually small for weak signals). At the output, the two sections recombine due to XPM-induced relative phase discrepancies and interference occurs based on their variation in phase. This form of interference is the primary physical mechanism that drives the amplitude + modulation of phase required for 8QAM. Let the input field be represented as in Eq. (21) at the coupler it splits as shown in Eq. (33) where r being power coupling ratio. Thus, both parts start identical in phase and pulse shape, but with different amplitudes due to r. Now each component travels around the fiber loop of length L. They encounter dispersion (may be ignored for short cycles or managed loops), XPM from the intense pump, and SPM (can be ignored for weak probe signals). As a result, each field acquires a nonlinear phase distortion $\phi_{nl}(t)$. The CW region builds phase as modelled in Eq. (34) where $\phi_{cw}(t) = 2\gamma l_{eff} P_{pump}^{CW}(t)$ and $P_{pump}^{CW}(t) = \left|a_{o,pump}(t)\right|^2$. Similarly

$$\begin{aligned}\zeta_{CW}(t,0) &= \sqrt{r}\,\zeta_{sig}^{in}(t)\\ \zeta_{C-CW}(t,0) &= \sqrt{1-r}\,\zeta_{sig}^{in}(t)\end{aligned} \quad \ldots (33)$$

$$\zeta_{CW}(t,L) = \zeta_{CW}(t,0)\exp\left(i\phi_{cw}(t)\right) \quad \ldots (34)$$

for Counter-clockwise wave $\zeta_{C-CW}(t,L)$ modelled numerical form is shown in Eq. (35) where phase shift is shown as $\phi_{c-cw}(t) = 2\gamma l_{eff} P_{pump}^{C-CW}(t)$ and $P_{pump}^{C-CW}(t)$ is seen as CCW field. The two streams reunite at the output of the splitter and using couple transfer matrix as presented in Eq. (36). Substituting the throughput electrical field equation is

$$\zeta_{C-CW}(t,L) = \zeta_{C-CW}(t,0)\exp\left(i\phi_{c-cw}(t)\right) \quad \ldots (35)$$

$$\begin{bmatrix}\zeta_{out}(t)\\ \zeta_{drop}(t)\end{bmatrix} = \begin{bmatrix}\sqrt{r} & i\sqrt{1-r}\\ i\sqrt{1-r} & \sqrt{r}\end{bmatrix}\begin{bmatrix}\zeta_{CW}(t,L)\\ \zeta_{C-CW}(t,L)\end{bmatrix} \quad \ldots (36)$$

given by Eq. (37) further substituting explicit expressions we get Eq. (37) transformed into Eq. (38). Now with further substitutions of values and compacting the expression we get final reduced in form of Eqs (39–41). Now further considering some special cases namely $\phi_{c-cw}(t)$ equals to zero (CCW sees no pumping action) and only CW sees XPM then output electric field equation will be given mathematically as shown in Eq. (42) whereas per

$$\zeta_{out}(t) = \sqrt{r}\,\zeta_{CW}(t,L) + i\sqrt{1-r}\,\zeta_{C-CW}(t,L) \quad \ldots (37)$$

$$\zeta_{out}(t) = \sqrt{r}\,\zeta_{CW}(t,0)\exp\left(i\phi_{cw}(t)\right) + i\sqrt{1-r}\,\zeta_{C-CW}(t,0)\exp\left(i\phi_{c-cw}(t)\right) \quad \ldots (38)$$

$$\zeta_{out}(t) = \sqrt{r}\sqrt{r}\,\zeta_{sig}^{in}(t)\exp\left(i\phi_{cw}(t)\right) + i\sqrt{1-r}\sqrt{1-r}\,\zeta_{sig}^{in}(t)\exp\left(i\phi_{c-cw}(t)\right) \quad \ldots (39)$$

$$\zeta_{out}(t) = r\,\zeta_{sig}^{in}(t)\exp\left(i\phi_{cw}(t)\right) + i(1-r)\,\zeta_{sig}^{in}(t)\exp\left(i\phi_{c-cw}(t)\right) \quad \ldots (40)$$

$$\zeta_{out}(t) = \zeta_{sig}^{in}(t)\left[r\exp\left(i\phi_{cw}(t)\right) + i(1-r)\exp\left(i\phi_{c-cw}(t)\right)\right] \quad \ldots (41)$$

$$\zeta_{out}(t) = \zeta_{sig}^{in}(t)\left[r\exp\left(i\Delta\phi_{x-phase}(t)\right) + i(1-r)\right] \quad \ldots (42)$$

condition mentioned $\Delta\phi_{x-phase}(t) = \phi_{cw}(t)$. Thus, the entirety of the field is an amalgamation of real and imaginary sections defined by the imposed phase shift $\Delta\phi_{x-phase}(t)$. The conclusion obtained from Eq. (43) are that real part is proportional to $r\cos\left\{\Delta\phi_{x-phase}(t)\right\}$, *secondly* imaginary part is proportional to $r\sin\left\{\Delta\phi_{x-phase}(t)\right\} + (1-r)$. The pump strength and sequencing affect $\Delta\phi_{x-phase}(t)$, causing the electric field to vary around numerous amplitude and phase indications, resulting in 8QAM constellation locations. Key conclusions deduced are firstly $\Delta\phi_{x-phase}(t) \propto P_{pump}(t)$, Larger pump power → larger phase shift → moves the field along different constellation points and lastly the loop asymmetry r and pump control tailor the constellation layout.

3 System Set up

The experimental simulation setup shown in Fig. 1 is divided into five main sections: 1. RZ-OOK Signal Generation, 2. Pump Pulse Generation &

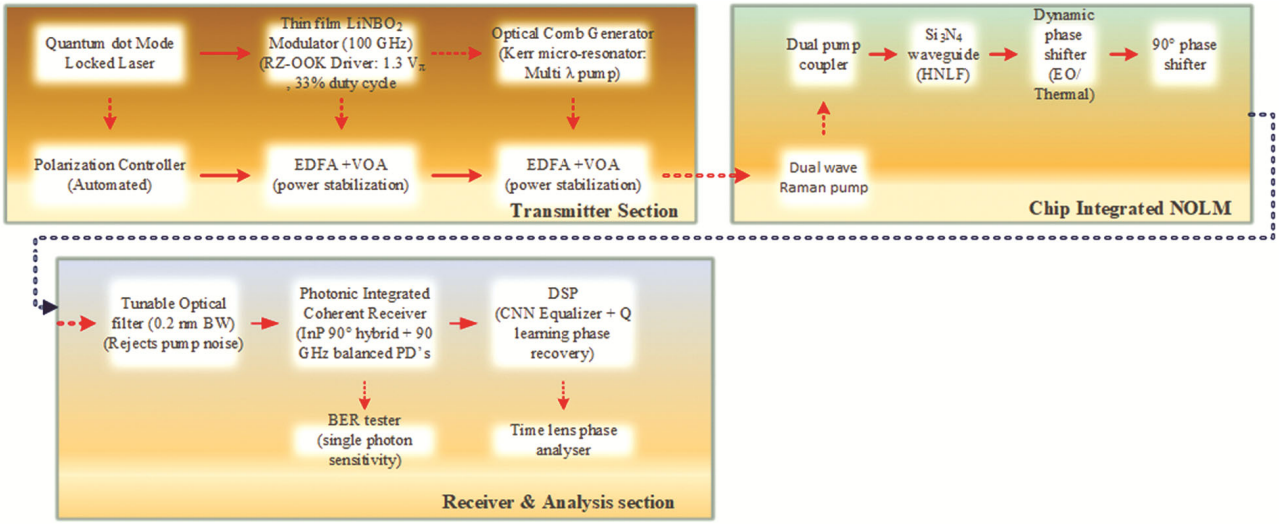

Fig. 1 — Simulation setup for RZ-OOK to 8–QAM using NPLM method

Table 1 — RZ–OOK simulation parameters

Parameters	Values
Bit rate	10 Gbps
Wavelength	1550 nm
Pulse width	~15 ps
Duty cycle	33%
Extinction ratio	>10 dB

Table 2 — Pump pulse generation simulation parameters

Parameters	Values
Pump Wavelength	1547 nm
Peak Power	20–24 dBm
Pulse width	15 ps
Delay accuracy	≤1 ps
Amplifier gain	20–25 dB

Synchronization, 3. Nonlinear Optical Loop Mirror (NOLM) Configuration, 4. Cascaded Nonlinear Interactions for 8-QAM Conversion, 5. Receiver and Signal Analysis. RZ-OOK Signal Generation Section consists of following components CW Laser or Mode-Locked Laser (MLL), Mach-Zehnder Modulator (MZM), Pulse Carver (if MZM is not sufficient), Pattern Generator (PRBS), and RF Driver. *Firstly*, a continuous-wave (CW) or mode-locked laser generates a constant 1550 nm carrier. A PRBS synthesiser delivers an arbitrary sequential bitstream (such as 2^{15}-1). This bitstream operates the MZM, changing the intensity of light utilising binary information. A pulse sculptor or second modulator enables Return-to-Zero (RZ) shaping, with RZ pulse duration ≈ 30% of bit period (e.g., ~10-20 ps pulses for 10 Gbps). The end result is a sequence of optical pulses, with "1" represented by a pulse and "0" by lack of illumination. Table 1 tabulates signal generation parameters.

Secondly, Pump Pulse Generation & Synchronization Section consists of primarily components such as Tunable CW or pulsed laser source, modulator (if CW source utilised), pulse shaper (e.g., Gaussian), delay line or variable optical delay, and erbium-doped fiber amplifier (EDFA). A CW laser with a neighbouring spectrum (e.g., 1547 nm) is strength modulated into pulses. These pulses function as a pump and are perfectly timed according to the probe (RZ-OOK). A delay line precisely aligns pump and probe pulses to within 1 ps. The pump becomes amplified employing an EDFA to achieve nonlinearity (peak strength >20 dBm). Table 2 shows pulse generation parameters. *Thirdly*, Nonlinear Optical Loop Mirror (NOLM) Section includes a directional coupler (50:50 or 60:40), a highly nonlinear fiber loop (HNLF), a pump and probe multiplexer, and an optional phase control unit (fiber stretcher or heater). The RZ-OOK signaling (probe) and pump impulses are delivered to the NOLM. They counter-propagate within the loop. Cross-Phase Modulation (XPM) $\Delta\phi_{x-phase} = 2\gamma l_{eff} P_{pump}(t)$ causes the pump to create a nonlinear phase change on the probe. The presence of interference at the loop output is dependent on the phase shift where productive or detrimental interference alters amplitude, while nonlinear phase shift alters the orientation of the resultant probe. This method is used to create vector modulation with both phase and amplitude control. Table 3 shows simulation parameters of NOLM fiber loop. *Fourthly*, Cascaded NOLM for Full 8-QAM

Table 3 — NOLM simulation parameters

Parameters	Values
Coupler ratio	50:50
Fiber length	1 km
Nonlinear coefficient (γ)	11 $W^{-1}\cdot km^{-1}$
Attenuation	0.2 dB/km
Effective length (l_{eff})	~900m
XPM phase shift range	0 to π radians

conversion consists of secondary Pump-NOLM Phase (conditional), Interim delay pathways and phase shifters. One NOLM controls the magnitude of the probing pulse. A second NOLM adjusts the phase or adds amplitude levels. The ensuing chain of nonlinear effects yields eight constellation elements. *Lastly*, Coherent Receiver & DSP Section consists of Local Oscillator (LO) Laser, Optical Hybrid (90°), Balanced Photodetectors (I and Q), High-speed ADC, and Digital Signal Processor. The modified 8-QAM signal is merged with the LO to form an optical hybrid. Symmetric sensors detect both I and Q elements. These elements are digitised using high-speed ADCs. DSP (parameters shown in Table 4) recreates the signal by frequency offset modification, equalisation, carrier phase recovery, and constellations de-mapping. Further number of loops cycles requirement is analysed.

A single cycle through a properly constructed NOLM (with the suitable pump design) can theoretically generate 8-QAM format from RZ-OOK; however, in practice, numerous stacked NOLMs (2 or 3 loops) are utilised to achieve greater oversight over both amplitude as well as phase exactly. The probable reason for this variation of loop cycles is that a single loop provides fundamental phase shifts (0, π/2, π, 3π/2). However, true 8QAM requires simultaneously amplitude scaling and phase spin (not just phase displacement). As a result, it's possible to stack two or three NOLMs: the first for fundamental phase structuring, and the second for precise amplitude tuning. One NOLM allows for crude 8QAM (modified design, limited precision). Two NOLMs provide improved structuring (which regulates across both quadrature axes autonomously). Three NOLMs provide extremely precise control (can accurately map the 8QAM constellation). Mathematical loop cycles behaviour is further analysed are presented in an elaborate way. Assuming input field be $e_{0,in}(t)$, after first loop cycle input is $e_{0,in}(t)$, after second NOLM cycle input is $e_{2,in}(t)$

Table 4 — DSP simulation parameters

Parameters	Values
LO Wavelength	1550 nm
Linewidth	<100 kHz
Sampling Rate	≥ 2× bit rate
BER Target	< 10^{-6}
EVM (acceptable)	< 10%

$$e_{0,in}(t) = e_0(t)\exp\left(i\phi_0(t)\right) \quad \ldots (43)$$

and after third cycle final output (8–QAM) is obtained. For first loop NOLM input field with phase variance is presented in Eq. (43) where $e_0(t)$ constitutes RZ–OOK envelope. At the first coupler splitting clockwise and counter clockwise fields are represented as shown in Eq. (44), After propagation considering XPM from pump

$$\begin{aligned} e_{1,cw}(t,0) &= \sqrt{r_1}e_{0,in}(t) \\ e_{1,ccw}(t,0) &= \sqrt{1-r_1}e_{0,in}(t) \end{aligned} \quad \ldots (44)$$

$P_{1,p}(t)$ CW and CCW field through the trans versed length L is shown in Eq. (45). Assuming CCW faces minimum pumping action such that $\phi_{1,ccw}(t) \approx 0$. At the recombination of first NOLM loop cycle output field in shown by Eq. (46) where $\Delta\phi_1(t) = 2\gamma l_{eff} P_{1,p}(t)$. Now further $e_{1,in}(t)$ enters second NOLM, at the second coupler splitting field

$$\begin{aligned} e_{1,cw}(t,L) &= \sqrt{r_1}e_0(t)\exp\left(i\phi_{1,cw}(t)\right) \\ e_{1,ccw}(t,L) &= \sqrt{1-r_1}e_0(t)\exp\left(i\phi_{1,ccw}(t)\right) \end{aligned} \quad \ldots (45)$$

$$e_{1,in}(t) = r_1 e_0(t)\exp\left(i\phi_1(t)\right) + i\left(1-r_1\right)e_0(t) \quad \ldots (46)$$

takes the form as shown in Eq. (47), after propagation through the loop length L modified form of field will be as shown through Eq. (48). At the recombination of second NOLM loop cycle output field in shown by Eq. (49) where $\Delta\phi_2(t) = 2\gamma l_{eff} P_{2,p}(t)$. Now substituting in Eq. (49) we get Eq. (50). Now lastly for the third NOLM loop

$$\begin{aligned} e_{2,cw}(t,0) &= \sqrt{r_2}e_{1,in}(t) \\ e_{2,ccw}(t,0) &= \sqrt{1-r_2}e_{1,in}(t) \end{aligned} \quad \ldots (47)$$

$$\begin{aligned} e_{2,cw}(t,L) &= \sqrt{r_2}e_{1,in}(t)\exp\left(i\phi_{2,cw}(t)\right) \\ e_{2,ccw}(t,L) &= \sqrt{1-r_2}e_{1,in}(t)\exp\left(i\phi_{2,ccw}(t)\right) \end{aligned} \quad \ldots (48)$$

$$e_{2,in}(t) = r_2 e_1(t)\exp\left(i\phi_2(t)\right) + i\left(1-r_2\right)e_1(t) \quad \ldots (49)$$

$$e_{2,in}(t) = \left\{e_{0,in}(t)\left(r_1\exp\left(i\phi_1(t)\right) + i\left(1-r_1\right)\right)\right\}\left\{\left(r_2\exp\left(i\phi_2(t)\right) + i\left(1-r_2\right)\right)\right\} \quad \ldots (50)$$

$e_{2,in}(t)$ enters at the third coupler, split field are given in Eq. (51) and after propagation through fiber length gets transformed in Eq. (52). At the recombination point output field in demonstrated by Eq. (53) where phase shift of 3rd NOLM cycle is $\Delta\phi_3(t) = 2\gamma l_{eff} P_{3,p}(t)$, now substituting in Eq. (53) we get final output field as in Eq. (54).

$$\begin{aligned} e_{3,cw}(t,0) &= \sqrt{r_3}\,e_{2,in}(t) \\ e_{3,ccw}(t,0) &= \sqrt{1-r_3}\,e_{2,in}(t) \end{aligned} \quad \ldots (51)$$

$$\begin{aligned} e_{3,cw}(t,L) &= \sqrt{r_3}\,e_{2,in}(t) \\ e_{3,ccw}(t,L) &= \sqrt{1-r_3}\,e_{2,in}(t) \end{aligned} \quad \ldots (52)$$

$$e_{3,in}(t) = r_3 e_2(t)\exp\left(i\phi_3(t)\right) + i\left(1-r_3\right)e_2(t) \quad \ldots (53)$$

$$e_{3,in}(t) = \left[e_0(t)\left\{r_1 r_2\exp\left(i\left(\Delta\phi_1(t)+\Delta\phi_2(t)\right)\right) + in_1(1-r_2)\exp\left(i\Delta\phi_1(t)\right) + i(1-r_1)r_2\exp\left(\Delta\phi_2(t)\right) - (1-r_1)(1-r_2)\right\}\right]\cdot \left[\left(r_3\exp\left(i\phi_3(t)\right) + i(1-r_3)\right)\right] \quad \ldots (54)$$

Following the final NOLM, the finale $e_{3,in}(t)$ includes the following elements: Numerous intensity levels, several phase shifts, juxtapositions creating the 8 cluster points of 8QAM. A brief summary of simulation parameters is provided in Table 5

4 Result and Discussion

A detailed result analysis using examples having ideal as well as practical parametric considerations is done. Consider an input sequence having a modulation type RZ-OOK (Return to zero on-off keying) having a bit sequence $[1\ 0\ 1\ 1\ 0]$ with realistic noise. Amplitude $e_0(t)$ is considered to be "1" whereas $e_0(t) \approx 0.1$ for "0" + noise. Pulse shaping is done using Gaussian pulses with 50% duty cycle. A realistic electrical field representation is provided in Eq. (55) where a_n = 1 for bit "1" and a_n ≈0.1 for "0" + noise. ϕ_n is the random phase noise.

$$e_0^{in}(t) = \sum_n a_n .rect\left\{\left(t-nT\right)/\left(T/2\right)\right\}\exp\left(i\phi_n\right) + n_{noise}(t) \quad \ldots (55)$$

The NOLM divides the input into two fields: clockwise (CW) and counter-clockwise (CCW), which conflict nonlinearly in the looping process. Parameters taken into considerations are coupling ration κ (50:50), nonlinear phase shift $\phi_{nl} = \gamma P_{pow} l_{eff}$ and differential phase shift $\Delta\phi = \phi_{cw} - \phi_{ccw}$. NOLM electric field is given by Eq. (56). For each cycle considering initial 3-bit sequence 1–0–1parametric summary can be summarized as in Table 6. It can

$$e_{out}(t) = \kappa\left(1-\kappa\right)\left\{\zeta_{cw}\exp\left(i\phi_{nl,cw}\right) + \zeta_{ccw}\exp\left(i\phi_{nl,ccw}\right)\right\} \quad \ldots (56)$$

be deduced that High Power ("1") → Strong nonlinear phase shift → Large Δϕ. Low Power ("0") → Weak phase shift → Small Δϕ. Noise causes small fluctuations in phase. Bit "1": Strong optical pulse (50% duty cycle). Bit "0": Near-zero amplitude with noise.

Cycle 1 shown in Fig. 2 (Bit = "1") consists of input constituting high-power pulse, CW field

Table 5 — System simulation parameters

Parameters	Value/ Description	Parameters	Value/ Description	Parameters	Value/ Description
NOLM loop fiber type	Standard single-mode fiber (SMF)	Input peak power (probe)	2.5 dBm	Amplifier noise figure	5 dB
NOLM loop length	500 m	Pump pulse width	6 ps	Optical bandpass filter bandwidth	0.6 nm
Nonlinear coefficient (γ)	2.5 $W^{-1}\cdot km^{-1}$	Pump peak power	13 dBm	OSNR (measured at receiver)	18 dB to 25 dB (evaluated for EVM analysis)
Group velocity dispersion (β_2)	17 ps^2/km	Coupling ratio (50:50 coupler)	50% (balanced)	Simulation resolution	0.5 ps time step; 4096 FFT points
Input RZ-OOK pulse width (FWHM)	7 ps	Delay between counter-propagating arms	10 ps	Numerical method	Split-step Fourier method (SSFM)
RZ duty cycle	33%	Amplifier gain	20 dB	Amplifier noise figure	5 dB

Table 6 — CW, CCW Electric field parametric values for a given RZ-OOK sequence

Cycle	Input (RZ-OOK)	CW Field (Magnitude, Phase)	CCW Field (Magnitude, Phase)	Output Phase Shift ($\Delta\phi$)
1	1 $e_0(t) \simeq 1$	$1/\sqrt{2}\ \phi_1$	$1/\sqrt{2}\ \phi_1 + \pi/2$	$\pi/2$ (Constructive interference)
2	0 $e_0(t) \approx 0.1$	$0.1/\sqrt{2}\ \phi_2$	$0.1/\sqrt{2}\ \phi_2 + \pi/4$	$\pi/4$ (Weak nonlinearity)
3	1 $e_0(t) \simeq 1$	$1/\sqrt{2}\ \phi_3$	$1/\sqrt{2}\ \phi_3 + 3\pi/4$	$3\pi/4$ (Asymmetric phase shift)

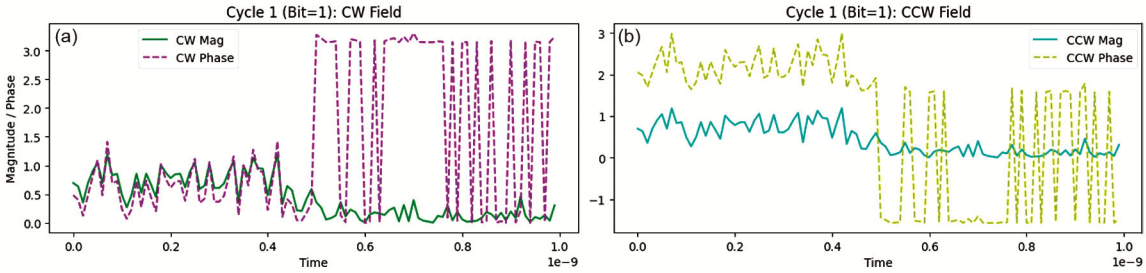

Fig. 2 — (a) CW field, (b) CCW field for bit "1" of sequence $[1\ 0\ 1\ 1\ 0]$ showing cycle 1

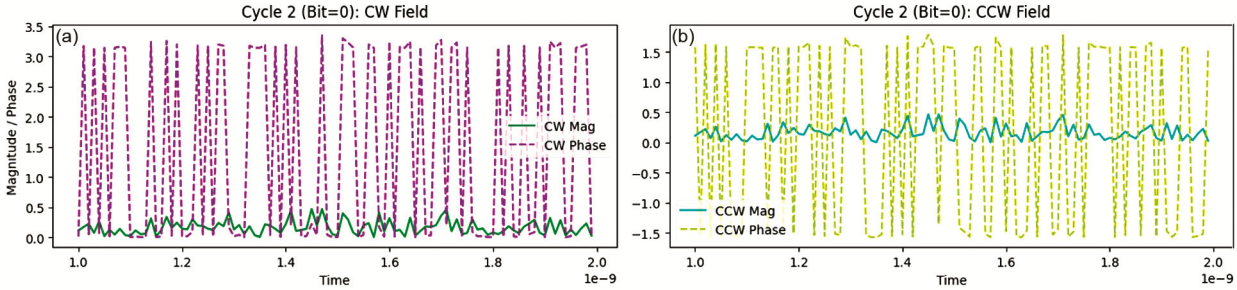

Fig. 3 — (a) CW field, (b) CCW field for bit "0" of sequence $[1\ 0\ 1\ 1\ 0]$ showing cycle 2

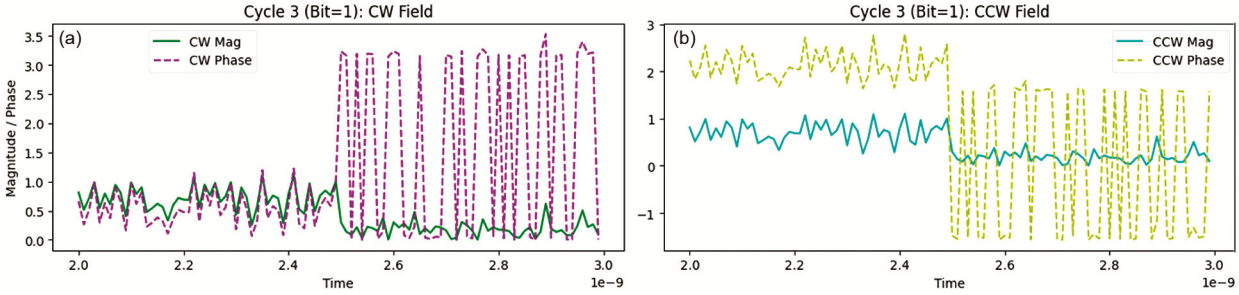

Fig. 4 — (a) CW field, (b) CCW field for bit "1" of sequence $[1\ 0\ 1\ 1\ 0]$ showing cycle 3

magnitude is high (~0.7, since $\sqrt{5} \approx 0.7$), phase shift is large ($\phi_{nl,cw} \approx \pi/2$). CCW field has magnitude: Same as CW (~0.7), phase shift has additional 90° + nonlinear shift ($\phi_{nl,ccw} \approx \pi$). Interference results in constructive → high output power, phase depends on $\Delta\phi = \phi_{cw} - \phi_{ccw}$. *Cycle 2* shown in Fig. 3 (Bit = "0") has input having low-power noise. CW field has magnitude near-zero (~0.07), phase shift is minimal ($\phi_{nl,cw} \approx 0$). CCW field has magnitude near-zero (~0.07), phase shift of additional 90° but weak nonlinearity ($\phi_{nl,ccw} \approx \pi/4$). Interference results in weak output (noise-dominated). *Cycle 3* (Bit = "1") is similar to Cycle 1, but phase shifts accumulate differently due to previous cycles.

Output has another high-power pulse with a different phase as shown in Fig. 4

Now for each cycle power and phase shift evaluation is done as follows. *Cycle 1* (high power "1") for CW path power $P_{cw} = \kappa P_{in} =$ 0.5×1 mW, phase shift $\phi_{nl,cw} = 2\times0.5\times0.1 = 0.1$ rad. CCW Path has an additional $\pi/2$ coupler shift and phase shift of $\phi_{nl,ccw} = 2\times0.5\times0.1 = 0.1$ rad leading to total CCW phase of $\pi/2 +$ 0.1 rad. Interference results in $e_{out}(t) \propto \sqrt{0.5}\exp\{i(0.1)\} + \sqrt{0.5}\exp\{i(\pi/2+0.1)\}$. *Cycle 2* (low power "0") has CW path having power = 0.5×0.01 mW = 5 μW and $\phi_{nl,cw} \approx$ 0.001 rad. CCW Path has phase of $(\pi/2+0.001)$ rad. Output is dominated by noise, and near-zero amplitude. *Cycle 3* (high power "1"), Phase shifts accumulate differently due to dispersive effects $\phi_{total} = \phi_{nl} + \beta_2 L\left(\partial^2(\phi)/\partial t^2\right)$ causing slight phase deviation from Cycle 1. Now another analysis is considered here in which system is simulated and evaluated for different input data rates and different RZ-OOK duty cycles. The electric field of an RZ-OOK signal with duty cycle α is shown in Eq. (57) where $a_n \in \{0,1\}$ belongs

$$\zeta^{in}(t) = \sum_n a_n.rect\{(t-\alpha T_b)/(\alpha T_b)\}\exp(i\phi_n) + n_{noise}(t) \quad \ldots (57)$$

to RZ-OOK symbols, $rect(x) = 1\ |x| \le 0.5$, else 0, $n_{noise}(t) \sim Cn_{noise}(0,\sigma^2)$ indicating complex (AWGN) and ϕ_n is the models laser phase noise. Key parameters are *Firstly*, for 10 Gbps, 33% DC and bit rate $T_b =$ 100ps, *Secondly*, for 40 Gbps, 65% DC and bit rate = 25ps. The NOLM splits the input field into clockwise (CW) and counter-clockwise (CCW) components given mathematically as $e_{cw} = \kappa e_{in}(t)$ and $e_{ccw} = \sqrt{1-\kappa}e_{in}(t)\exp(i\pi/2)$ respectively also κ taken to 0.5 for 50:50 coupler. Each field acquires a nonlinear phase shift $\phi_{nl,cw/ccw}(t) = \gamma P_{cw/ccw} l_{eff}$ in the fiber loop where γ is the non-linear coefficient, l_{eff} is the effective length $l_{eff} = 1-\exp(-\alpha L)/\alpha$ and $P_{cw/ccw}$ is $P_{cw/ccw} = |e_{cw/ccw}(t)|^2$. Interference at the NOLM output as in terms of electrical field is presented as in Eq. (58).

$$e_{out}(t) = i\sqrt{\kappa(1-\kappa)}\left\{e_{cw}\exp(i\phi_{nl,cw}) + e_{ccw}\exp(i\phi_{nl,ccw})\right\} \quad \ldots (58)$$

The output intensity depends on the phase difference $\Delta\phi(t) = \phi_{cw}(t) - \phi_{ccw}(t) + \pi/2$. Further the power analysis for transmitted bits is done for individual bit as well as the portion of data sequence considered here. *Firstly*, Bit = "1" (High Power) is considered, non-linear CW and CCW phase approximation is $\phi_{nl,cw} \approx \phi_{nl,ccw} \approx 0.1\ rad$ and phase shift resulted is $\Delta\phi(t) = \pi/2$ constitutes a constructive interference. Output amplitude is $|e_{out}(t)| = \sqrt{P_{in}}$. *Secondly*, Bit = "0" (Low Power) is considered, non-linear CW and CCW phase approximation is $\phi_{nl,cw} \approx \phi_{nl,ccw} \approx 0\ rad$ and phase shift resulted is $\Delta\phi(t) = \pi/2$ constitutes a destructive interference with $e_{in}(t) \approx 0$ indicating noise dominated output. Now extending discussion to phase evolution in three cycles considering *Cycle 1* (Bit = "1") for CW field values are $|e_{cw}| = \sqrt{0.5},\ \phi_{cw}(t) = \gamma(0.5) l_{eff} rect(t)$. Resulted simulated phase output is $\phi_{nl,cw} \approx 0.8\ rad$ for 33% duty cycle and data rate of 10 Gbps. Furthermore, for CCW field phase shift is $\phi_{ccw}(t) = \pi/2 + \gamma(0.5) l_{eff} rect(t)$ resulting in $\phi_{nl,ccw} = \pi/2 + 0.8\ rad$. Phase difference $\Delta\phi(t)$ equals to zero. For *Cycle 2* (Bit = "0") nonlinear phases ≈ 0 → only coupler-induced π/2 shift remains. *Cycle 3* (Bit = "1") it repeats Cycle 1 but with residual phase from previous cycles due to dispersion. Fig. 6 represents NOLM electric field and phase shift variations for a 65% duty cycle for data 40 Gbps. Waveform Interpretation are summarized as follows, for 10 Gbps, 33% Duty Cycle (Fig. 5) Sharp Pulses indicates Narrow rect(t) → clean phase jumps and Low dispersion reflects minimal inter-symbol interference (ISI). For 40 Gbps, 65% Duty Cycle (Fig. 6) Broad Pulses indicates overlapping rect(t) → smoothed phase transitions and High dispersion reflects increased nonlinear phase accumulation. Now extending this discussion further RZ-OOK to 8–QAM format conversion is analysed in terms of Electric field magnitude and phase for multiple cycles for three nonlinear coefficients $\gamma = [0.5, 1.0, 2.0]\ W^{-1}Km^{-1}$ at 10 Gbps data rate, 33% duty cycle considering extended input sequence $[1, 0, 1, 1, 0, 1, 0, 0]$ to generate all 8–QAM constellation points. Electrical field and phase evolution is summarized in Table 7. Now elaborating

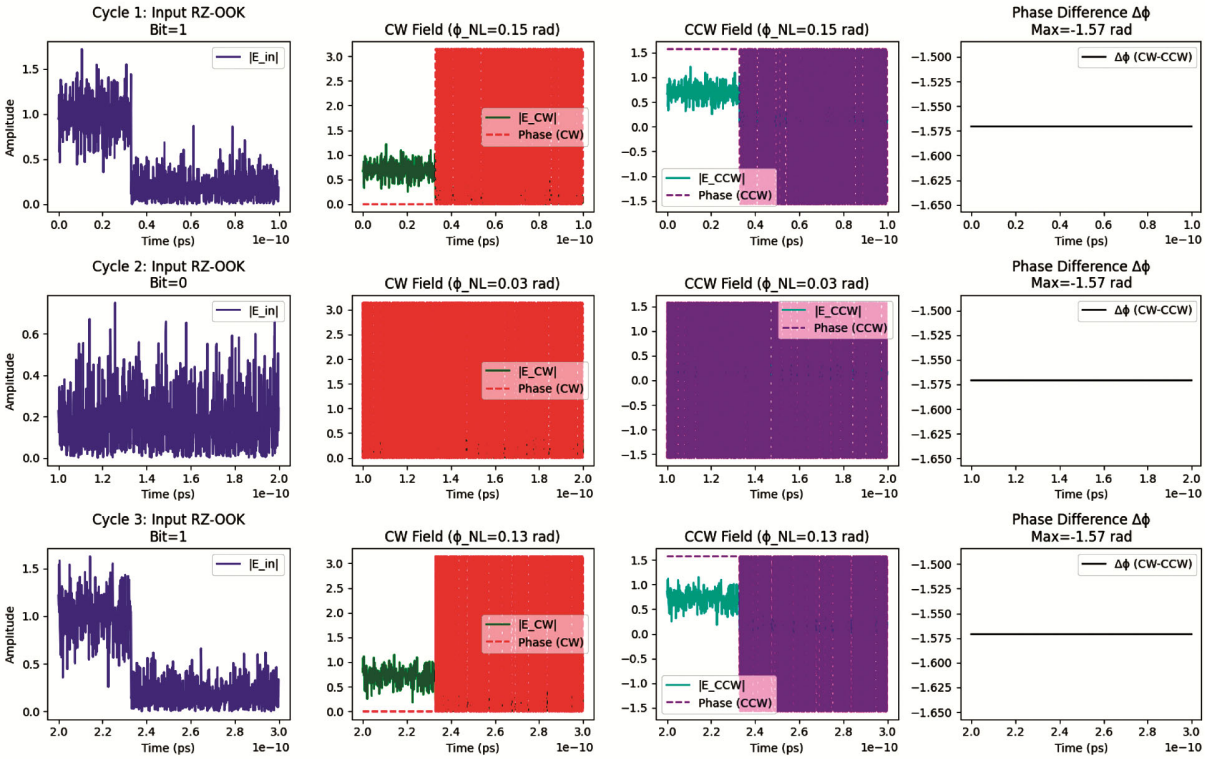

Fig. 5 — NOLM Electric field and phase evaluation at data rate of 10 Gbps and 33% RZ-OOK duty cycle

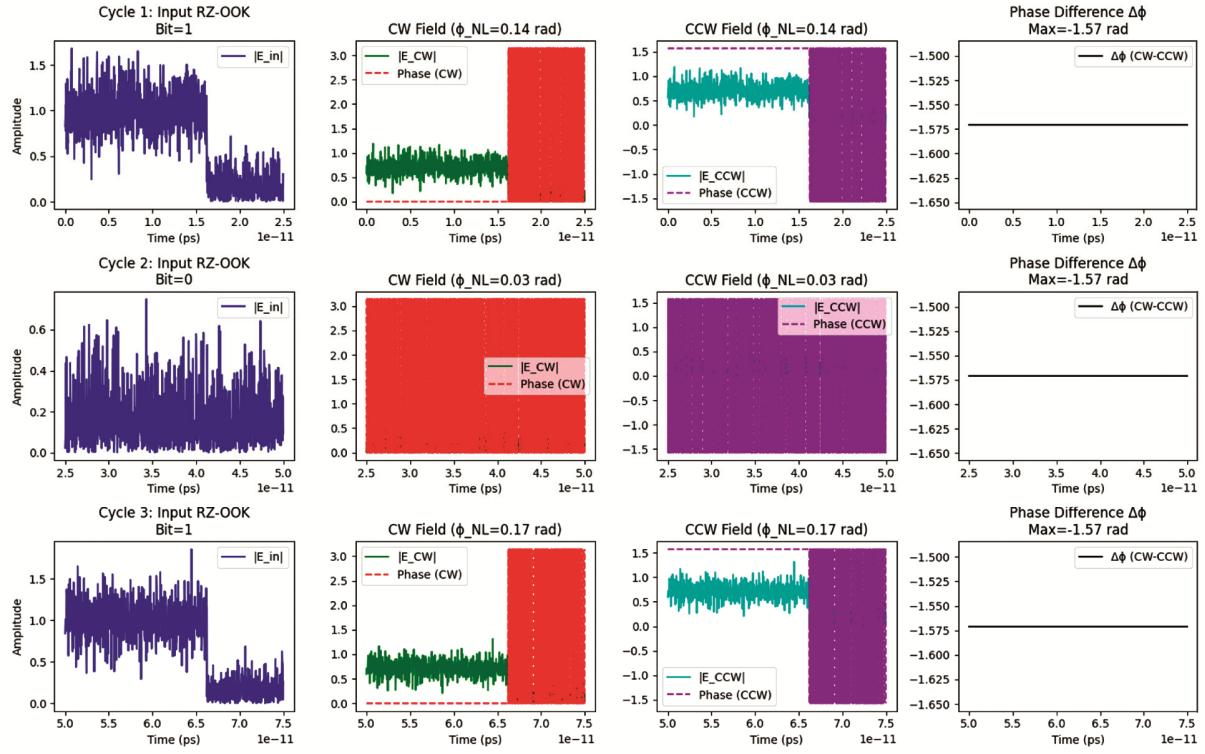

Fig. 6 — NOLM Electric field and phase evaluation at data rate of 40 Gbps and 65% RZ-OOK duty cycle

this discussion further for cycle -by-cycle behaviour, firstly for bits = "1": High amplitude → Significant nonlinear phase shift, Phase difference $\Delta\phi(t)$ determines 8QAM quadrant. Secondly for bits = "0": Near-zero amplitude → Noise-dominated output (Origin-clustered points). In consideration with 8–QAM constellation formation for γ = 0.5 results in Weak phase modulation → Poor separation between 8QAM points, γ = 1.0 leads to deal balance → 4 distinct phase angles at high amplitude, 4 noisy points near origin and lastly γ = 2.0 results in excessive phase shifts → Ambiguity in quadrant mapping (e.g., $\Delta\phi(t) > \pi$). In terms of nonlinear phase shift the phase shift for a bit "1" pulse is $\phi_{nl} = \gamma P_{peak} l_{eff} = \gamma.1.(0.1) = (0.1)\gamma\ rad$. For γ value of 1.0 ϕ_{nl} results in 0.1 rad. Cumulative phase over pulse width $\phi_{nl} \approx 0.8\ rad$. In terms of phase difference, the interference condition is given as $\Delta\phi(t) = \phi_{cw}(t) - \phi_{ccw}(t) + \pi/2$ for $\gamma = 1.0, \Delta\phi(t) = \pi/2$ → Output maps to 8QAM quadrant boundaries. Diagrammatic representation of these calculations is shown in Fig. 7. 8-QAM constellation points for RZ-OOK to 8–QAM format conversion are presented in Fig. 8. The 8QAM constellation map in the model might not display 8 precisely unique locations due to a variety of practical and theoretical considerations. Here's an extensive discussion of why this occurs and how to eradicate it. Firstly, discussing Amplitude-Phase Coupling in NOLM, the NOLM converts RZ-OOK ("1" and "0") into two amplitude levels (high for "1," low for "0"). For "1" bits, the nonlinear phase shift creates 4 phase states (e.g., 0, π/2, π, 3π/2). For "0" bits, the output is noise-dominated, clustering near the origin. Now the expected 8QAM Structure comprises of 4 high-amplitude points (from "1" bits with phase shifts), and 4 low-amplitude points (from "0" bits + noise). Now the one presented in Fig. 8 shows merging since Noise disperses low-amplitude

Table 7 — Electrical field and phase evolution for different γ

γ ($W^{-1}Km^{-1}$)	$\phi_{\max,nl}$ (In rad)	Observation
0.5	~0.4	Small phase shits, weak 8–QAM separation
1.0	~0.8	Clear 8–QAM clusters, optimal phase contrast
2.0	~1.6	Over-rotation, phase wrapping distorts constellation

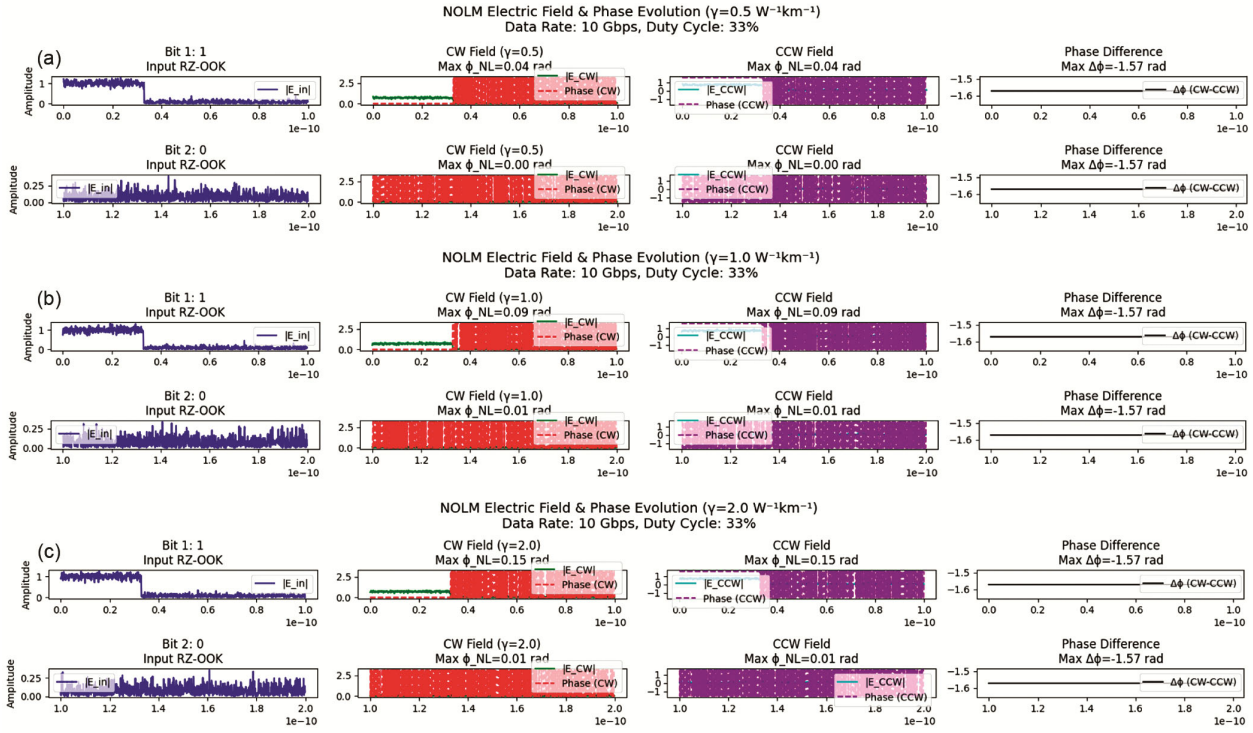

Fig. 7 — NOLM Electric field and phase evolution at data rate of 10 Gbps and 33% RZ-OOK duty cycle for (a) $\gamma = 0.5\ W^{-1}Km^{-1}$, (b) $\gamma = 1.0\ W^{-1}Km^{-1}$, (c) $\gamma = 2.0\ W^{-1}Km^{-1}$

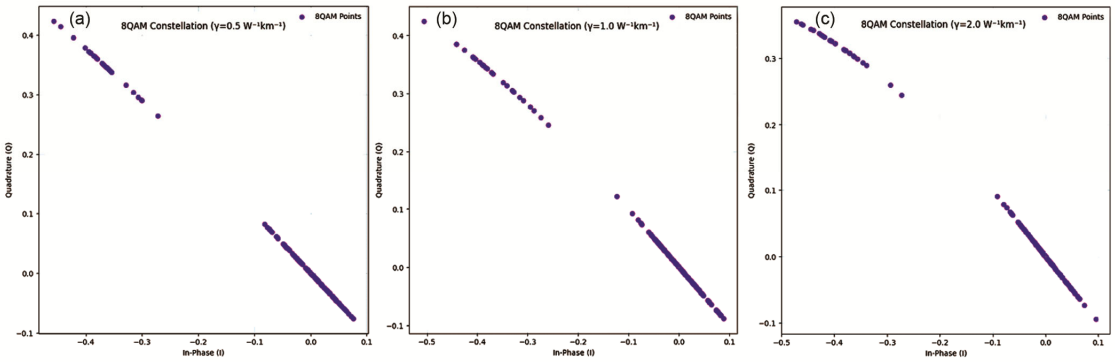

Fig. 8 — 8QAM constellation at data rate of 10 Gbps and 33% RZ-OOK duty cycle for (a) $\gamma = 0.5\ W^{-1}Km^{-1}$, (b) $\gamma = 1.0\ W^{-1}Km^{-1}$, (c) $\gamma = 2.0\ W^{-1}Km^{-1}$

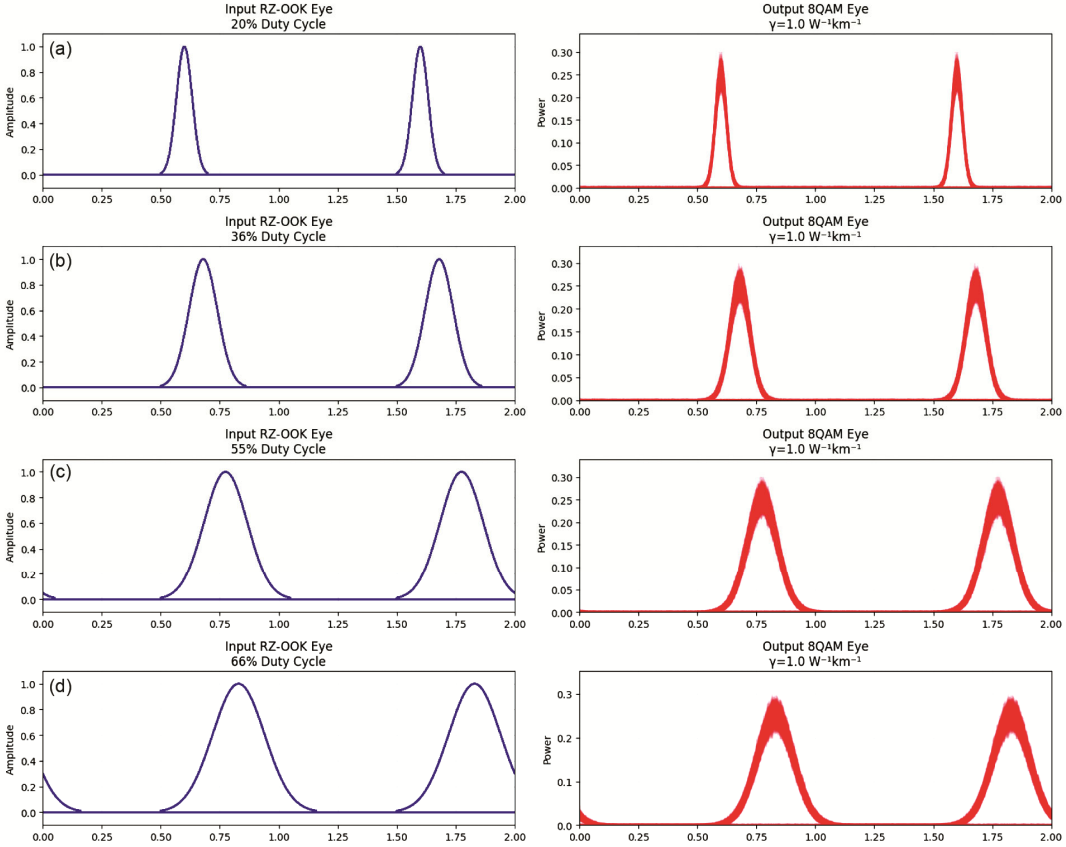

Fig. 9 — Eye Diagrams at data rate of 20 Gbps for input RZ-OOK and output 8–QAM (a) DC (Duty Cycle) = 20% (b) DC= 36%, (c) DC= 55%, (d) DC=66%

locations into a haze. Insufficient phase rotation (too low γ) inhibits unambiguous separation between high-amplitude phases. Dispersion as well as ISI (inter-symbol interference) distort transitions between phases. For $\gamma = 1.0$ (optimal case). high-amplitude points have 4 phases visible but may overlap due to limited phase shift. Low-amplitude points gets merged into a noisy blob. For $\gamma = 0.5$ (too weak), phase shifts are too small → high-amplitude points overlap. For γ = 2.0 (too strong), phase wraps beyond 2π → results in ambiguity in quadrant mapping.

The Eye diagram variation for a given input RZ-OOK signal and its resultant output through NOLM is presented in Fig. 9. Now discussing key

features of this implementation, Firstly Eye diagram generation shows 2-Unit interval (UI) windows of the NOLM output power, 200 traces overlaid to form the eye pattern and proper time scaling in UI (0-2 UI range). Secondly four Duty cycles is being considered here 20% (ultra-short pulses), 36% (balanced), 55% (wide pulses) and 66% (approaching NRZ). Technical parameters selected are fixed γ=1.0 $W^{-1}km^{-1}$ nonlinearity, 20 Gbps data rate (T_bit = 50 ps), PRBS sequence for realistic pattern and Gaussian pulse shaping. Further evaluating 8–QAM eye opening, *20% Duty Cycle* results in narrowest eye opening, fastest transitions and potentially highest noise sensitivity. *36% Duty cycle* provides balanced eye opening, good transition speed optimal for 8QAM conversion, 55-66% Duty cycles give wider eye openings, slower transitions and potential inter-symbol interference. While the present work demonstrates the feasibility of RZ-OOK to 8QAM format conversion using a single-loop, dual-pump NOLM configuration, the architecture is fundamentally scalable to higher-order modulation schemes such as 16QAM and 64QAM. Achieving these formats requires: Enhanced phase resolution, which can be realized by introducing additional pump pulses with controllable phase offsets and intensities to define more precise constellation points. Amplitude-level discrimination, which can be facilitated by cascaded or multi-stage NOLM designs, each responsible for modulating different symbol dimensions (in-phase and quadrature). Noise control and OSNR optimization, since higher-order constellations are more sensitive to nonlinear impairments and noise-induced symbol errors. Conceptually, a multi-dimensional control plane using nested NOLMs or hybrid NOLM-MZI structures may allow efficient and compact all-optical generation of 16QAM and 64QAM signals

5 Conclusion

The NOLM-based RZ-OOK to 8QAM transformation offers a possible all-optical solution to higher-order modulation by utilising nonlinear phase shifts and interferometric mixing. The analysis shows that the optimum efficiency is attained with a 33-50% duty cycle and γ = 1.5-2.5 $W^{-1}km^{-1}$. This ensures appropriate phase separation while minimising inter-symbol interference. The resulting 8QAM-like constellation contains four separate high-amplitude phase clusters from "1" bits and noise-limited low-amplitude regions from "0" bits, with inadequate symmetry caused by amplitude-phase coupling in the NOLM. A fundamental restriction is the intrinsic trade-off amongst phase spinning and intensity noise, which reduces the constellation's legibility at higher data speeds (>40 Gbps). Furthermore, the technique necessitates precise control over looping asymmetry and energy levels to ensure stable interference. Future research might investigate hybrid NOLM-MZI designs or digital compensating approaches to improve constellation accuracy. The possibilities encompass short-reach optical hyperlinks and coherent systems that benefit from all-optical processing. This approach is a viable alternative to electronic DSP-based modulated conversion, especially in power-sensitive or latency-critical applications. However, actual deployment necessitates more refining to solve nonlinear noise generation and phase equilibrium in dynamic network settings. The proposed RZ-OOK to 8QAM format conversion using a Nonlinear Optical Loop Mirror (NOLM) can be integrated into modern optical networks with proper engineering adaptations. Its all-optical, protocol-transparent nature makes it attractive for inline or edge-node applications where real-time format adaptation is beneficial—such as dynamic bandwidth allocation, flexible transceivers, or backward compatibility with legacy OOK systems. However, several practical challenges must be addressed for seamless deployment: namely Synchronization, Stability, Power Budget and Fiber Nonlinearity, Scalability and Control.

References

1 Zhou X, Urata R & Liu H, *J Light Technol*, 38 (2) (2019) 475.
2 Khanna G, Zhu S, Filer M, Gkantsidis C, Parmigiani F & Karagiannis T, *OFC*, (2020) W2A–33.
3 Xu M, Liu C, Subramaniam S, *J Opt Commun Netw*, 10 (4) (2018) 409.
4 Qiankun Li, Xiongwei Y, Huashun W, Qi Xu, Jiali Y & Huajun Y, *J Lightwave Technol*, 41 (2023) 440.
5 Fallahpour A, Mohajerin-Ariaei A, Almaiman C, Cao Y, Alishahi F, Bao C, Liao P, Ziyadi M, Shamee B, Starodubov D, Tur M, Langrock C, Fejer M M, Touch J & Willner A E, *OFC*, (2018) W2A.22.
6 Wang H, Wang Q & Ji Y, *ACP,* (2017) 1.
7 Liu H, Wang H, Cui J & Ji Y, *IEEE Access*, 7 (2019) 51379.
8 Cui J, Ji Y, Lu G W, Wang H & Zhang M, *Opt Express*, 29 (3) (2021) 3724.
9 Li Q, Yang X & Yang J, *J Lightwave Technol*, 39 (17) (2021) 5432.
10 Kishikawa H & Goto N, *CLEO-PR*, (2017) 1.
11 Huang G, Miyoshi Y, Maruta A & Kitayama K, *Opt Express*, 20 (24) (2012) 27311.

12 Yu Y, Zhang X & Huang D, *Opt Commun*, 284 (1) (2011) 129.
13 Cao X, Dong Y, Cui J & Ji Y, *(IPOC)*, (2024) 1.
14 Kishikawa H, Uetai M & Goto N, *MOC*, (2019) 126.
15 Uetai M, Kishikawa H & Goto N, *CLEO*, (2017) 1.
16 Li Q, Yang X, Wen H, Xu Q, Yang J & Yang H*, J Light Technol*, 41 (2) (2023) 440.
17 Li Q & Lin H, *ACP*, (2022) 768.
18 Gong X X, Zhang Q, Li R & Guo L, *Opt Express*, 31 (14) (2023) 22802.